Planetary and Space Science 60 (2012) 297–303

Contents lists available at SciVerse ScienceDirect

Planetary and Space Science

journal homepage: www.elsevier.com/locate/pss

IBEX-Lo observations of energetic neutral hydrogen atoms originating from the lunar surface

D.F. Rodríguez M. [a,*], L. Saul [a], P. Wurz [a], S.A. Fuselier [b], H.O. Funsten [c], D.J. McComas [d], E. Möbius [e]

[a] Physics Institute, University of Bern, Sidlerstrasse 5, 3012 Bern, Switzerland
[b] Space Physics Department, Lockheed Martin Advanced Technology Center, 3251 Hanover Street, Palo Alto, CA 94304, USA
[c] Los Alamos National Laboratory, Los Alamos, New Mexico, USA
[d] Southwest Research Institute, San Antonio, TX 78228-0510, USA and University of Texas at San Antonio, San Antonio, TX 78249, USA
[e] Space Science Center and Department of Physics, University of New Hampshire, 39 College Road, Durham, NH 03824, USA

ARTICLE INFO

Article history:
Received 26 March 2011
Received in revised form
16 September 2011
Accepted 17 September 2011
Available online 6 October 2011

Keywords:
Energetic neutral atoms
ENAs Moon albedo
Solar wind
IBEX-Lo

ABSTRACT

In this paper we present quantitative results of observations of energetic neutral atoms (ENAs) originating from the lunar surface. These ENAs, which are hydrogen atoms, are the result of the solar wind protons being reflected from and neutralised at the surface of the Moon. These measurements were made with IBEX-Lo on NASA's IBEX satellite. From these measurements we derive the energy spectrum of the ENAs, their flux, and the lunar albedo for ENAs (i.e., the ratio of ENAs to the incoming solar wind protons). The energy spectra of the ENAs clearly show that their origin is directly from the solar wind via backscattering, and that they are not sputtered atoms. From several observation periods we derived an average global albedo of $A_H = 0.09 \pm 0.05$. From the observed energy spectra we derive a generic spectrum for unshielded bodies in the solar wind.

1. Introduction

NASA's Interstellar Boundary Explorer (IBEX) mission was designed to investigate the interaction of the heliosphere with the surrounding interstellar medium via the observation of Energetic Neutral Atoms (ENAs) from a near Earth vantage point (McComas et al., 2004, 2009a). IBEX recorded the first all-sky maps of ENAs produced by the interaction of the heliosphere with the local interstellar medium at heliocentric distances of ~100 AU (McComas et al., 2009b; Funsten et al., 2009a; Fuselier et al., 2009a; Schwadron et al., 2009). The IBEX spacecraft was launched on 19 October 2008 and is currently in an elliptical, near-equatorial Earth orbit of $\sim 3 \times 50 R_E$ (Earth radius). The IBEX payload consists of two single-pixel ENA sensors with large geometric factors, IBEX-Lo (Fuselier et al., 2009b) and IBEX-Hi (Funsten et al., 2009b), and a single Combined Electronics Unit (CEU) that controls these sensors, stores data, and is the payload interface to the spacecraft bus (McComas et al., 2004, 2009a).

Because the Moon has no atmosphere or strong magnetic field to protect its surface from external influences, the solar wind directly interacts with the lunar surface. The solar wind ions are partially absorbed by the lunar regolith but a significant fraction of them is scattered back to space, with most of these backscattered particles being neutralised in the process to form energetic neutral atoms (ENAs). The first measurements of ENAs coming from the Moon and the first determination of the global efficiency for backscatter and neutralization (the lunar ENA albedo) were determined using observations above ~300 eV from IBEX-Hi as ~10% (McComas, et al., 2009c). Measurements made with the Sub-keV Atom Reflecting Analyser (SARA) instrument (Barabash et al., 2009) onboard the Indian Chandrayaan-1 spacecraft orbiting the Moon in a 100 km lunar orbit subsequently gave an albedo of $A_H = 0.16$–0.20 at the lunar equator in the energy range above 100 eV (Wieser et al., 2009).

These large fractions of reflected and neutralised solar wind challenged previous assumptions about almost complete adsorption of solar wind ions impinging on the lunar surface (Wieser et al., 2009). The observations of the backscattering and neutralisation processes of solar wind on the lunar surface are important for the analysis of plasma interaction with the lunar surface, which is also important for all other celestial bodies that have no atmosphere.

2. Instrumentation

The IBEX-Lo sensor is a single pixel, large geometric factor camera (Fuselier et al., 2009b). It detects 10 eV–2 keV neutral atoms from the heliosphere and from the interplanetary medium in 8 broad energy bands. The IBEX-Lo sensor uses surface

* Corresponding author. Tel.: +41 31 631 8546; fax: +41 31 631 4405.
E-mail address: diego.rodriguez@space.unibe.ch (D.F. Rodríguez M.).

0032-0633/$ - see front matter © 2011 Elsevier Ltd. All rights reserved.
doi:10.1016/j.pss.2011.09.009

reflection and conversion to convert neutrals into negative ions (Wurz, 2000) and then accelerates the ions so that they can be deflected away from the viewing direction to efficiently suppress background from ambient particles and photons (Wurz et al., 2009). The ions are energy and mass analysed and registered with high efficiency. The sensor uses a triple coincidence TOF mass spectrometer, which separates hydrogen, helium, and oxygen. The sensor has undergone stringent tests and calibrations that have demonstrated that it meets the requirements for the IBEX mission. The IBEX-Lo and IBEX-Hi sensors view perpendicular to the spin axis of the spacecraft and the spin axis is always directed within a few degrees of the Sun. Thus, as the spacecraft spins, the single pixel cameras view a swath of the sky $\sim 7^\circ \times 360^\circ$. This swath is divided into sixty 6° angular bins.

3. Observations

There are only selected time periods during a few orbits when the Moon is in the field-of-view (FOV) of the IBEX sensors. These time periods are predicted from the spacecraft and Moon ephemeris. To determine what orbits could be used to observe the Moon, we used several selection criteria. Preferably both the Moon and IBEX are outside the terrestrial magnetosphere, i.e., outside the magnetopause. Also, the lunar signal should not interfere with ENA fluxes of the heliospheric Ribbon (McComas et al., 2009b), the Interstellar Neutrals (ISN) (Möbius et al., 2009), or the magnetosphere. Unfortunately, these restrictions meant that not all the orbits where the Moon was in the FOV were finally chosen for further analysis. The above criteria were used to select the orbits 29, 43, 44, 47, 58 and 72. However, for the orbits 43 and 44 the Moon was in the magnetosheath, which will be discussed separately.

3.1. Extraction of background

Fig. 1 shows IBEX orbit 58 and the nominal location of the Moon's orbit and the Earth's bow shock and magnetopause. IBEX observed the Moon near apogee, when it was well outside the Earth's bow shock. In the direction opposite the Moon, IBEX-Lo observed Interstellar Neutrals (which are observed by IBEX from December to February).

Fig. 2 shows the data from IBEX-Lo for all energy channels for orbit 58. This figure is a spin angle–time spectrogram showing the triple coincidence hydrogen events over the 360° spin angle (vertical axis, labelled Spin Phase ranging from 0 to 1) over about 6 days of the ~ 8 day IBEX orbit (horizontal axis in decimal days). The Spin Phase from 0 to 1 corresponds to the Spin angle of $0–360^\circ$, where 0° points toward the ecliptic North Pole, and the Earth's ram direction is at spin phase 0.75. The ISN signal is seen at ~ 0.75 spin phase, which is nearly in the ecliptic. The Moon is in the FOV from day 721.6 to 722.2 nearly opposite the ISN direction (out of the ecliptic direction because of the Moon's 5° orbit tilt relative to the ecliptic and the IBEX orbit's $\sim 11^\circ$ tilt relative to the Earth's equator).

To remove the background from the signal in the selected orbits, we took samples from two rectangular areas of equal size to the area containing the lunar signal. In Fig. 2 the background is defined by the green boxes namely BG1, BG2 and the red box is for the lunar signal. By subtracting these background counts directly from the raw signal we achieve good accounting of the background source (Wurz et al., 2009). By organising the data in a matrix of spin phase versus day of year, we chose areas both

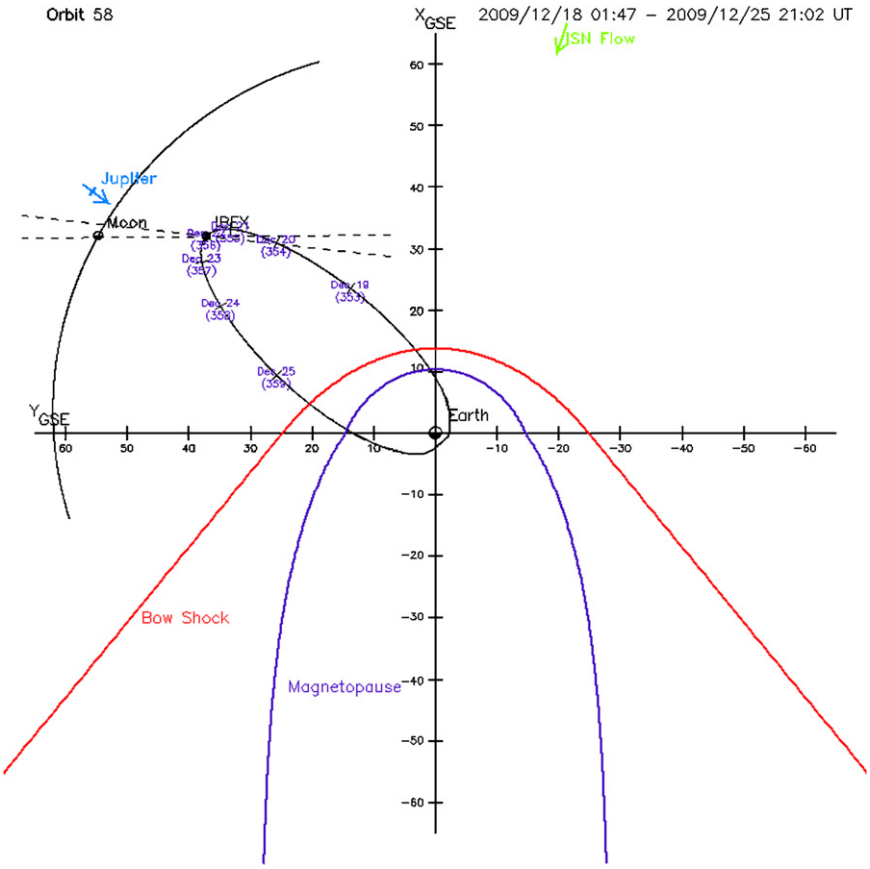

Fig. 1. Shows an ecliptic plane projection of IBEX orbit 58 with the location of major magnetospheric boundaries, the Moon orbit, and the IBEX FOV in the plane. Note that the ISN signal arrives in the direction opposite the Moon.

above and below the location of the lunar signal, because these are highly representative of the background collected in the same time range in Day of Year (DOY) of the signal. Often there is a background by high energy particles observed at all spin angles, which is easily accounted for using the background areas above and below. The lunar signal in orbit 72 suffers from a strong background, and varying with spin phase because it is located very close to the signal of ENAs from the ISN. The areas chosen to determine the background rate for the lunar viewing of this orbit are not located above and below the signal but before and after the lunar signal to correctly remove the background arising from the ISN. As example, we showed in Fig. 2 the boxes BG3 and BG4. The details of observation time and the spin phase of the lunar signal are summarised in Table 1, which also shows the number of the orbit, the time range in Day of Year (DOY). It also shows the ranges of Spin Phase, both to determine the signal and the background, which was subsequently removed.

After removing background, the lunar signal was corrected for cross-talk from other energy bins. Each of the eight energy bins receives a contribution from the higher energy bins, due to sputtering of H atoms from the conversion surface. This effect falsely increases the number of events counted in each of the energy bins. To correct for this cross-talk and derive the actual number of events in each bin, we must remove events added from each of the higher bins. The energy bin 8 (1.9 keV) is the highest energy bin of IBEX-Lo; it does not receive any contribution from this process, since we assumed that the signal is produced by solar wind energy (~1 keV) protons, and used for each analysed orbit an average solar wind speeds; in contrast, bin 1 receives input from all the higher energies. To perform the correction, we used the matrix given in Table 2. These values were calculated from laboratory calibration data of the relative geometrical factors for various energy bins. These laboratory measurements used nearly mono-energetic neutral atom beams to determine the relative contributions in each energy bin.

In Table 2, each column defines an energy bin as indicated and each row of the table shows the relative contribution from the higher energy bins that we have to correct for. For example, for bin 1 the first row indicates the numbers to multiply the value of events to that bin; has a value of 1 because this does not add anything to itself, the next row in the same column represents the contribution from bin 2 to bin 1, which must be subtracted from the previous value. The next row shows the contribution from bin 3, which must be subtracted from the previous residual and so on, leading eventually to the adjusted signal to bin 1. This process was done with each of the energy bins of IBEX-Lo.

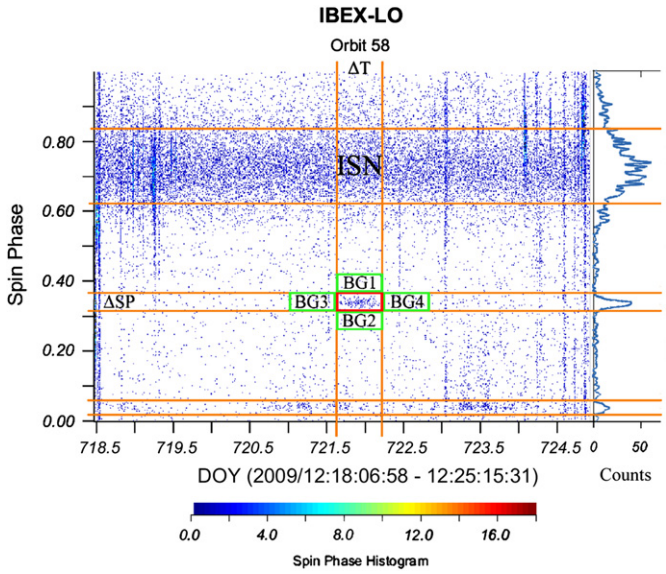

Fig. 2. A summed spin angle–time spectrogram of ENAs signal recorded by IBEX-Lo during orbit 58. The Moon enters the IBEX-Lo FOV, during 21–22 December 2009 when the Moon crosses IBEX's FOV. Both the Moon and the IBEX are outside the magnetosphere. The ENA signal originating from the lunar surface is clearly seen in the range of Day of Year 2008 (DOY) 721.6–722.2 and at the Spin Phase of IBEX-Lo between 0.32 and 0.370. The signal is found well separated from the ISN signal, which in this case it can be seen as a wide horizontal strip across the graph between 0.6 and 0.8 in Spin Phase (nearly in the ecliptic plane). For this orbit, the lunar signal was observed away from strong background sources. The right panel shows a histogram of counts for the time period when the Moon is inside IBEX-Lo's FOV. The small signal observed of spin phase ~0.02–0.05 is a background signal appearing in most IBEX-Lo observations.

3.2. Lunar ENA flux

To calculate the ENA flux from the lunar surface from the corrected counts of an observation recorded by the IBEX-Lo

Table 2
Values of relative geometric factor that must be used to correct the counts in each energy bin to generate the corrected number of events. Each column shows how this bin receives additions from all energy bins higher than itself.

Relative geometrical factor							
E bin 1 14 eV	**E bin 2 27 eV**	**E bin 3 52 eV**	**E bin 4 102 eV**	**E bin 5 197 eV**	**E bin 6 451 eV**	**E bin 7 908 eV**	**E bin 8 1903 eV**
1	0	0	0	0	0	0	0
0.523	1	0	0	0	0	0	0
0.0859	0.4[a]	1	0	0	0	0	0
0.0225	0.05[a]	0.28	1	0	0	0	0
0.0213	0.03[a]	0.0552	0.3[a]	1	0	0	0
0.0216	0.03[a]	0.0399	0.05[a]	0.3795	1	0	0
0.0235	0.0209	0.0314	0.0549	0.107	0.334	1	0
0.0216	0.00752	0.0254	0.0451	0.0541	0.107	0.304	1

[a] These values are interpolated. The nominal *H* centre energies of each energy bin are given in the header.

Table 1
IBEX orbits selected for our study. The asterisk (*) in the orbit 72 indicates that the rectangular areas taken as background are on the sides of the area of the signal in contrast to other orbits, where the background areas were chosen above and below the moon signal.

Orbit number	Signal				Background							
	DOY range since 1 January 2008		Spin phase range		DOY range since 1 January 2008				Spin phase range			
29	502.5	503.0	0.68	0.730	502.5		503.0		0.63	0.68	0.730	0.78
43	609.0	609.6	0.26	0.300	609.0		609.6		0.22	0.26	0.300	0.34
44	616.6	617.8	0.69	0.750	616.6		617.8		0.63	0.69	0.750	0.81
47	637.0	637.8	0.26	0.305	637.0		637.8		0.22	0.26	0.300	0.34
58	721.6	722.2	0.32	0.370	721.6		722.2		0.27	0.32	0.370	0.42
72*	829.2	829.9	0.68	0.720	828.5	829.2	829.9	830.6	0.68		0.720	

sensor we consider the following relationship:

$$Flux_i^{IBEX} = \left(\frac{Cts_i^{adj}}{GF_i^{dig}}\right)\Omega_{FoV}\frac{\Delta E}{E}\frac{DF}{\Delta T} \quad (1)$$

We have defined the flux received by IBEX in each energy bin i as $Flux_i^{Ibex}$ with Cts_i^{adj} the corrected counts for the events in each energy bin, and the geometric factor GF_i^{dig} for each energy bin for hydrogen atoms using the triple coincidence detection. The geometric factor of the instrument was obtained in the laboratory calibration (Fuselier et al., 2009b), with an additional adjustment from post-launch calibration (McComas et al., 2009b).

The solid angle Ω_{FOV} given by the instrument field-of-view (FOV) is defined as

$$\Omega_{FoV} = 2\pi(1-\cos\phi_{FoV}) \quad (2)$$

with the opening angle ϕ_{FOV} of the IBEX-Lo FOV equal to 6.54° FWHM (Fuselier et al., 2009b), which corresponds to a resolution in spin phase of $\Delta SP_{IBEX\text{-}Lo}=0.018$. This value is constant for all orbits. During the IBEX lunar observations the average of angular size of the Moon is in the range of 0.25–0.87°, thus if was always much smaller than the angular resolution of IBEX-Lo. Therefore only global observations could be performed.

The energy resolution is $\Delta E/E=0.8$, and the value of the Duty Factor DF is defined as

$$DF = 8\left(\frac{SP_{total}}{\Delta SP_{signal}}\right) \quad (3)$$

where the value of 8 represents the number of energy bins of IBEX-Lo and the quantity in the parentheses is the amount of time observing the Moon during a given spin. This quantity is determined by dividing the total Spin Phase or maximum SP_{total} (by definition has a value of 1, and 0 for the spin phase minimum), by the fraction of the Spin Phase ΔSP_{signal} for the lunar signal (see Fig. 2), which varies for each orbit. The Duty Factor, DF, is divided by the length of time of signal collection ΔT, measured in seconds.

Knowing the ENA fluxes, $Flux_i^{Ibex}$, for each energy bin of IBEX-Lo, in addition to the distance of the IBEX satellite from the Moon r_{Ibex}, we can deduce the ENA flux produced at the lunar surface for each energy bin by

$$Flux_i^{Moon} = Flux_i^{IBEX}\left(\frac{2\pi}{\Omega_{Moon}}\right)\left(\frac{1+\cos\phi_{sw}}{2}\right)^{-1} \quad (4)$$

The second term on the right hand side of Eq. (4) accounts for the fact that only a fraction of ENAs emitted from the IBEX-facing hemisphere is in the direction of IBEX. Here, we calculate the solid angle of the Moon as seen from IBEX.

$$\Omega_{Moon} = 2\pi(1-\cos\theta), \quad \text{with } \theta = \arctan\left(\frac{r_{Moon}}{r_{IBEX}}\right) \quad (5)$$

where the distances r_{Moon}, and the IBEX spacecraft location at a distance r_{Ibex} from the centre of the Moon, are known from orbit data. This term includes the inverse square dependence on distance from the source, and further assumes that the ENA emission function from the lunar surface is isotropic with emission angle. These simplifying assumptions, along with the assumption of isotropic flux emission over lunar position, are used because we are concerned here with a global measurement of ENA flux. The observations are too far away for more detailed considerations of the ENA flux dependencies using IBEX-Lo. The third term on the right hand side of Eq. (4) accounts for the fact that only a fraction of the Moon is "illuminated" by the solar wind ions when viewed from a different direction than the solar wind flow direction, with ϕ_{SW} the angle between the solar wind and ENA directions (see Fig. 3).

When the Moon is outside the magnetosphere (orbits 29, 47, 58 and 72) the observation angle is $\phi_{SW}\sim 90°$ with respect to the solar wind direction; thus only half of the Moon visible to IBEX is

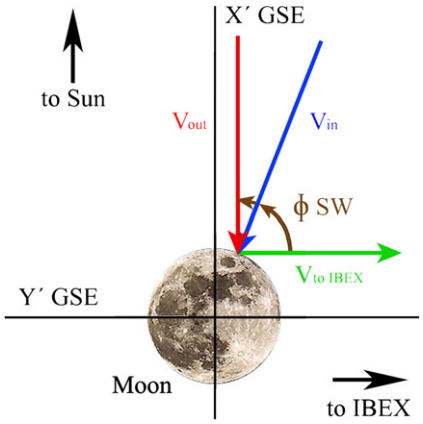

Fig. 3. Shows the directions of the solar wind speed incident on the lunar surface, the red arrow shows the direction when the Moon is outside the magnetosphere V_{out}, a 90° with the IBEX axis (green arrow). The blue arrow V_{in} indicates the direction of the velocity when the Moon is in the magnetosphere, one would expect that had an angle ϕ_{SW} to the vertical different to 90° (see Table 3). (For interpretation of the references to colour in this figure legend, the reader is referred to the web version of this article.)

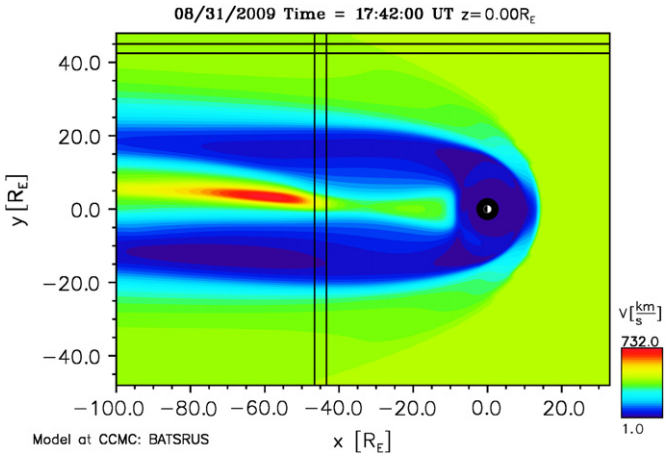

Fig. 4. Shows the results of the simulation of the plasma velocity in the magnetosphere based on data taken by the ACE satellite for the date of the IBEX orbit #43. The area defined by the intersection of the lines determines the approximate position of the Moon for the lunar ENA observations during that orbit. The xy-plane is shown. The Moon was downstream of the bow shock on the flanks, where the solar wind heating, slowing, and deflection are minimal.

illuminated by solar wind ions. The actual angle varies as the spacecraft moves and so an average is taken over the observing time. The error produced from this procedure is much less than the others considered in the calculation described herein ($<5\%$). When the Moon is inside the bow shock or magnetosphere (orbits 43 and 44) the observation angle is different ($\phi_{SW}\neq 90°$); see Fig. 3. Also the plasma parameters, i.e., the density and flow velocity, are different from the solar wind plasma parameters. So we had to analyse these observations in a different way than done for the orbits where the Moon is in the solar wind. This analysis was done with the help of the BATS-R-US, a magnetosphere model of Community Coordinated Modeling Center (CCMC).

BATS-R-US, the Block-Adaptive-Tree-Solarwind-Roe-Upwind-Scheme, was developed by the Computational Magnetohydrodynamics (MHD) Group at the University of Michigan, now Center for Space Environment Modeling (CSEM). It was designed using the Message Passing Interface (MPI) and the Fortran90 standard and executes on a massively parallel computer system (Gombosi et al., 2004). For this model we used the solar wind plasma data from the ACE satellite (McComas et al., 1998; Smith et al., 1998) as input values. The results for orbit 43 are shown in Figs. 4 and 5,

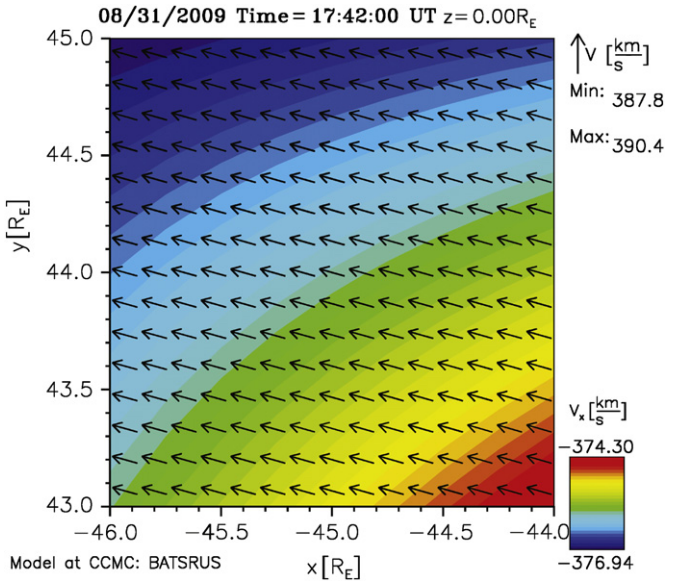

Fig. 5. Shows the simulation magnitude of plasma velocity of the magnetosphere to 43 of IBEX's orbit, for the area indicated in Fig. 4. Overlaid arrows show the direction of the plasma velocity in the *xy*-plane. The plasma flow is dominantly in the *xy*-plane, with the magnitude of the velocity being close to the solar wind values measured by SOHO to the same orbit, see Table 3.

Table 3
Shows the average values of some plasma parameters used in the simulation with **BATS-R-US** for the orbits of IBEX in comparison to data collected with SOHO, and shows the angle ϕ_{SW} of incidence.

Orbit number	SOHO			BATS-R-US			ϕ_{SW} [deg.]
	Energy [eV]	Energy standard deviation	V_{SW} [km/s]	Energy [eV]	Energy standard deviation	V [km/s]	
29	783.7	66.52	387.31	–	–	–	~90
43	836.3	78.57	400.35	790.61	3.92	389	~75.4
44	489.6	37.11	306.32	659.69	4.03	356	~78.0
47	527.1	32.18	317.86	–	–	–	~90
58	649.0	89.37	352.69	–	–	–	~90
72	1634.8	35.76	559.74	–	–	–	~90

using the Day of Year (DOY), to find the plasma parameters of the solar wind flow at the same time made by the PM sensor on the SOHO satellite (Ipavich et al., 1998).

The results from the magnetosphere model show the plasma behaviour for the area in which the Moon was located when we observed the lunar ENAs with IBEX. The plasma velocity in the observations of orbit 43 is slightly lower than those obtained for the solar wind plasma outside the bow shock. For both orbits, the incidence angle was obtained through the vector components of velocity. The results for orbits 43 and 44 are lower but close to $\phi_{SW}=90^{\circ}$. These results are given in Table 3. With the magnetosphere model we have all the input parameters to analyse orbits 43 and 44 in the same way as the orbits when the Moon was in the solar wind.

From the Eq. (1), we calculated the ENA fluxes in each IBEX-Lo energy bin for the selected orbits. The calculated ENA fluxes in units of $cm^{-2}\,s^{-1}$ are shown in Fig. 6 as function of centre energy for each of the eight energy bins. The indicated errors are from full error propagation of Eq. (1) where counting statistics and the uncertainty in absolute geometric factors (which is 30%) are the major contributors. The ENA fluxes are roughly constant in the range from about 30 eV up to an energy near the solar wind energy. Above the solar wind energy, the ENA fluxes drop steeply.

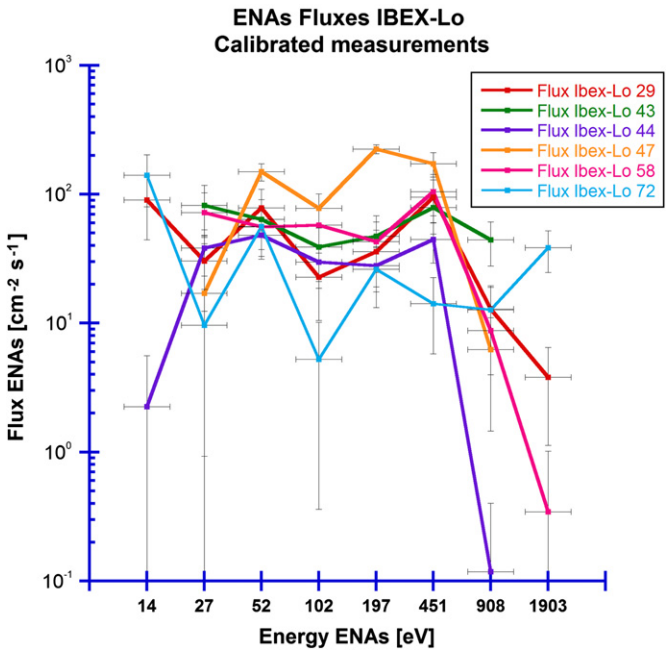

Fig. 6. ENA flux as function of energy for all selected orbits. For orbits 43 and 44 the Moon was in the magnetosheath. For the other orbits the Moon was in the solar wind. Only signals are plotted when enough counts were available after accounting for background and cross-talk between energy bins. Horizontal error bars indicate the energy resolution of the instrument.

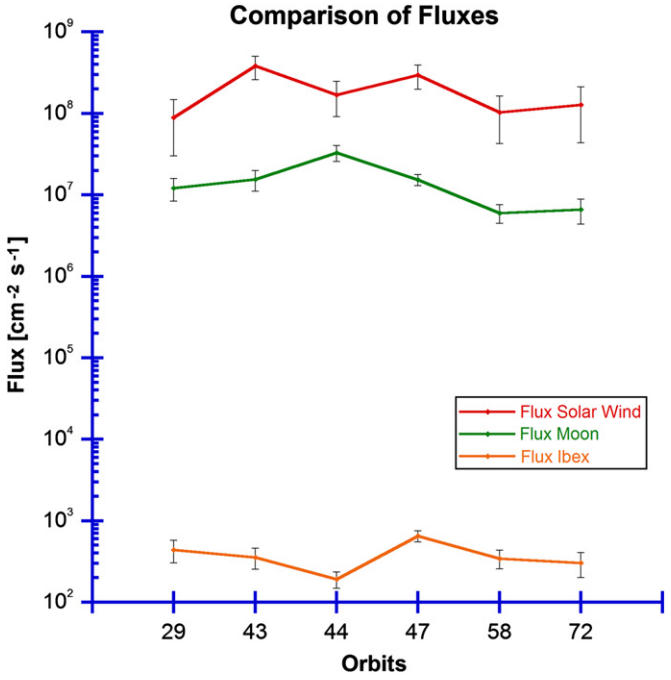

Fig. 7. Total fluxes of solar wind proton, lunar ENAs observed at the IBEX location, and ENA fluxes released from the lunar surface. Error bars shown are from of the propagation of error.

A similar energy dependence is observed for all orbits. These ENA energy spectra are very similar to earlier observations: IBEX-Hi had energy coverage from 380 eV to 6 keV (McComas et al., 2009c) and the SARA instrument on Chandrayaan-1 had an energy coverage from 40 eV to 3 keV (Wieser et al., 2009).

Energy integrated ENA fluxes from the Moon are shown in Fig. 7 for all investigated orbits. The indicated errors of the ENA

fluxes are from error propagation of the counting statistics and the uncertainty in the geometric factor (Fuselier et al., 2009b). The error bars of the solar wind data are a combination of the uncertainty in the instrument calibration and of the solar wind fluctuation during the measurement interval.

From the emitted lunar ENA fluxes we can make an estimate of the ENAs lunar albedo if we know the incident solar wind flux on the surface of the Moon $Flux_{SW}$. To find these values we used data from ESA's SOHO satellite and from the simulation with BATS-R-US, and knowing the exact dates and times of the observations by IBEX-Lo (see Table 1). Using the values of the density of solar wind protons n_{SW}, and its velocity v_{SW}, and the solar wind flux $Flux_{SW}=v_{SW}\,n_{SW}$, we get the flux of solar wind protons that were converted to ENAs on the lunar surface and were subsequently detected by IBEX-Lo. These calculations allow for the time delay in measuring the solar wind, due to the distance they must travel from the location of the SOHO spacecraft prior to impact on the Moon, as well as the time it takes for the neutrals to travel from the lunar surface to IBEX.

With these values, we calculate the ratio of the emitted lunar ENA flux compared to the incident solar wind flux for each IBEX orbit by taking the sum, $\Sigma Flux_i^{Moon}$, over the energy bins of the ENAs fluxes of IBEX-Lo that were emitted from the lunar surface over the solar wind flux, using the SOHO and BATS-R-US plasma data for the respective orbits (Fig. 8). We obtained the average of this flux ratio (average global ENA albedo) over all orbits, which is 0.09 ± 0.05. This ratio can be considered as global ENA albedo. The derived value of the global albedo is limited to the range of energy bins covered by the IBEX-Lo sensor, although we can assume that most of the lunar ENA flux is registered by IBEX-Lo based on the energy spectra (see Fig. 6), in contrast with the IBEX-Hi energy sensitivity (McComas et al., 2009a, s2009b, 2009c). The value for the global ENA albedo is an average value for the lunar surface since the angular size of the Moon during the IBEX observations is smaller than the angular resolution of IBEX-Lo. Thus, inhomogeneities of the surface composition or texture possibly resulting in a variation of the local ENA albedo are not resolved in these measurements. Also any details of the angular distribution of the scattering function at the lunar surface require observations from a much closer vantage point.

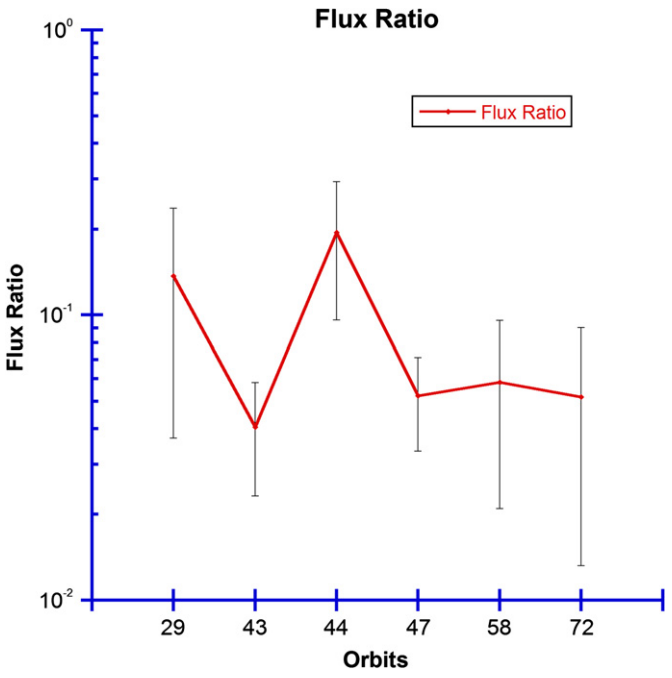

Fig. 8. Ratio of lunar ENA flux to impacting solar wind flux for the different orbits of IBEX-Lo. The error bars come from propagation of statistical error.

4. Discussion and conclusions

We report observations of lunar hydrogen ENAs over the full IBEX-Lo energy range down the lowest energy bin (14 eV centre energy, spanning from 10 to 18 eV). This means that IBEX-Lo almost completely covers the energy spectrum of the ENAs from the lunar surface for typical solar wind speeds < 500 km/s. Fig. 9 shows the data of all measurements normalised to the solar wind energy and normalised solar wind flux. These observations of lunar ENAs show roughly a flat energy spectrum extending down to small fractions of the solar wind energy. Toward higher energies the ENA spectrum rolls over around the solar wind energy, and essentially no ENA fluxes are observed above the solar wind energy considering the uncertainty in the ENA energy determination and the variability of the solar wind velocity during the observation interval (see horizontal error bars in Fig. 9). From the data in Fig. 9 we derive a mathematical formulation for a generic energy spectrum, $g\,(E_{ENA}/E_{SW})$, for ENAs scattered from the lunar surface, where we have chosen a simple function to reproduce the observations

$$g(E_{ENA}/E_{SW}) = \frac{Flux_{ENA}(E_{ENA})}{Flux_{SW}} = 0.031\exp\left(\frac{3.18}{\ln(E_{ENA}/E_{SW})-1.61}\right) \quad (6)$$

with E_{ENA}/E_{SW} the ratio of the energy of the ENAs to the solar wind energy. Fig. 9 also shows the energy response of IBEX-Lo instrument, which we used to deconvolve the generic energy spectrum.

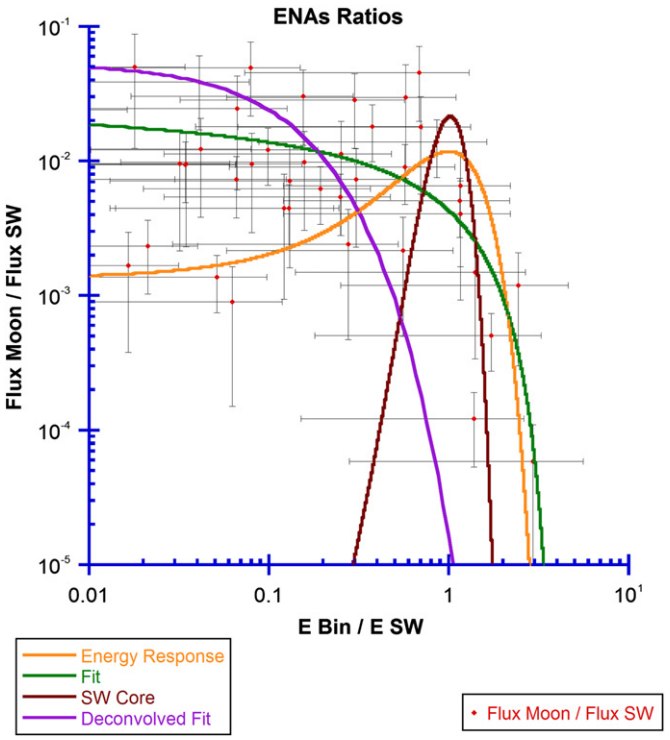

Fig. 9. Flux ratio of all measurements of all orbits. Vertical error bars are from error propagation of Eq. (1), mostly from counting statistics and uncertainty in the geometric factor of IBEX-Lo. Horizontal error bars account for the IBEX-Lo energy resolution and solar wind variability during the observations. For comparison the core solar wind distribution is shown (with Mach number 10), and a distribution with a FWHM equal to that of the IBEX-Lo Energy response, both normalised to the observed flux ratio at the solar wind energy. The solid green line shows the best fit to our generic ENA spectrum described in the text; brown line, the deconvolution of the fit energy response. (For interpretation of the references to colour in this figure legend, the reader is referred to the web version of this article.)

The deconvolved energy spectrum shows that on average no ENAs are observed above the solar wind energy.

Particle scattering has been studied extensively in the laboratory (e.g. Niehus et al., 1993). In the laboratory, significant fractions of reflected particles have only been observed for flat surfaces. However, when scattering particles from laboratory surfaces under bombardment by mono-energetic ion beams significantly different energy spectra are observed compared to scattering from the lunar surface. The laboratory spectra are peaked at the incoming energy of the particle (with a small energy loss) and with a long tail toward lower energies (Scheer et al., 2005, 2006). One explanation for this difference in the energy spectra is that the lunar surface is rough, leading to more frequent multiple scatterings. However, the high fraction of reflected particles cannot be understood in that case.

We observed also the behaviour of the variable energy H-ENA albedo (Flux Ratio), correlated with the solar wind. In our study with IBEX-Lo we determine a total global value for the flux ratio, with an average flux ratio of $A_H \approx 0.09 \pm 0.05$, which is compatible with the earlier measurements of the global albedo based on IBEX-Hi data of $A_H \sim 0.1$ (McComas et al., 2009c), and the local value of $A_H = 0.16$–0.20 at the lunar equator derived by Wieser et al. (2009), from Chandrayaan-1/SARA data. The study of data from the lunar hydrogen ENAs, i.e., the backscattered and neutralised solar wind, is very relevant to planetary science since many planetary surfaces are not shielded from the influence of the solar wind, and these ENAs are a source of energetic hydrogen atoms in the solar system. We can conjecture that the generic spectrum of lunar ENAs (Eq. (6)) represents a typical spectrum of ENAs emitted from unshielded planetary bodies covered with a mineral regolith surface.

Acknowledgements

We gratefully acknowledge provision of the IBEX data by the IBEX team and IBEX Science Operations Center (ISOC), the IBEX-Lo cross talk matrix by Lee W. Petersen, Uni. New Hampshire, and the IBEX orbits plots by Steve Petrinec. Simulation results of magnetosphere have been provided by the Community Coordinated Modeling Center (CCMC) at Goddard Space Flight Center through their public runs on request system (http://ccmc.gsfc.nasa.gov). The CCMC is a multi-agency partnership between NASA, AFMC, AFOSR, AFRL, AFWA, NOAA, NSF and ONR. The BATSRUS with RCM Model was developed by the Dr. Tamas Gombosi et al. at the CSEM. Solar wind data from the ACE is provided by the SWEPAM team. Work on this study by the U.S. authors was supported by the IBEX mission as a part of NASA's Explorers program.

References

Barabash, S., Bhardwaj, A., Wieser, M., Sridharan, R., Kurian, T., Varier, S., Vijayakumar, E., Abhirami, V., Raghavendra, K.V., Mohankumar, S.V., Dhanya, M.B., Thampi, S., Kazushi, A., Andersson, H., Yoshifumi, F., Holmström, M., Lundin, R., Svensson, J., Karlsson, S., Piazza, D., Wurz, P., 2009. Investigation of the solar wind–Moon interaction onboard Chandrayaan-1 mission with the SARA Experiment. Current Science 96 (4), 526–532.

Funsten, H.O., Allegrini, F., Bochsler, P., Dunn, G., Ellis, S., Everett, D., Fagan, M., Fuselier, S.A., Granoff, M., Gruntman, M., Gurthie, A., Hanley, J., Harper, R., Heirtzler, D., Janzen, P., Kihara, K., King, B., Kucharek, H., Manzo, M., Maple, M., Mashburn, K., McComas, D.J., Möbius, E., Nolin, J., Piazza, D., Pope, S., Reisenfeld, D.B., Rodriguez, B., Roelof, E.C., Saul, L., Turco, S., Valek, P., Weidner, S., Wurz, P., Zaffke, S., 2009a. The interstellar boundary explorer high energy (IBEX-Hi) neutral atom imager. Space Science Review 146, 75–103.

Funsten, H.O., Allegrini, F., Crew, G.B., DeMajistre, R., Frisch, P.C., Fuselier, S.A., Gruntman, P., Janzen, M., McComas, D.J., Möbius, E., Randol, B., Reisenfeld, D.B., Roelof, E.C., Schwadron, N.A., 2009b. Structures and spectral variations of the outer heliosphere in IBEX energetic neutral atom maps science 326 (5955), 964–966. doi:10.1126/science.1180927.

Fuselier, S.A., Allegrini, F., Funsten, H.O., Ghielmetti, A.G., Heirtzler, D., Kucharek, H., Lennartsson, O.W., McComas, D.J., Möbius, E., Moore, T.E., Petrinec, S.M., Saul, L.A., Scheer, J., Schwadron, N., Wurz, P., 2009a. Width and variation of the ENA flux ribbon observed by the interstellar boundary explorer. Science 326, 962–964.

Fuselier, S.A., Ghielmetti, A.G., Hertzberg, E., Moore, A.S., Isaac, D., Hamilton, J.W., Tillier, C., Moebius, E., Granoff, M.S., Heirtzler, D., King, B., Kucharek, H., Longworth, S., Nolin, J., Turco, S., Ellis, S., Googins, J., Kudirka, F., Tyler, J., Vosbury, M., Clark, G., O'Neal, M., Wurz, P., Scheer, J.A., Saul, L.A., Piazza, D., Bochsler, P., Wieser, M., Schlemm, C., McComas, D.J., Scherrer, J., Pope, S., Funsten, H.O., Chornay, D., Lobell, J., Moore, T.E., Rosmarynowski, P., Friedmann, T., Nemanich, R.J., 2009b. The IBEX-Lo sensor. Space Science Review 146, 117–147.

Gombosi, T., Powell, K.G., De Zeeuw, D.L., Clauer, C.R., Hansen, K.C., Manchester, W.B., Ridley, A.J., Roussev, I.I., Sokolov, I.V., Stout, Qu.F., Tóth, G., 2004. Solution adaptive MHD for space plasmas: Sun-to-Earth simulations. Computing in Science and Engineering 6 (2), 14–35.

Ipavich, F.M., Galvin, A.B., Lasley, S.E., Paquette, J.A., Hefti, S., Reiche, K.-U., Coplan, M.A., Gloeckler, G., Bochsler, P., Hovestadt, D., Grünwaldt, H., Hilchenbach, M., Gliem, F., Axford, W.I., Balsiger, H., Bürgi, A., Geiss, J., Hsieh, K.C., Kallenbach, R., Klecker, B., Lee, M.A., Managadze, G.G., Marsch, E., Möbius, E., Neugebauer, M., Scholer, M., Verigin, M.I., Wilken, B., Wurz, P., 1998. The solar wind proton monitor on the SOHO spacecraft. Journal of Geophysical Research 103, A, 17205–17214.

McComas, D.J., Bame, S.J., Barker, P., Feldman, W.C., Phillips, J.L., Riley, P., Griffee, J.W., 1998. Solar wind electron proton alpha monitor (SWEPAM) for the advanced composition explorer. Space Science Reviews 86, 563–612.

McComas, D.J., Allegrini, F., Bochsler, P., Bzowski, M., Collier, M., Fahr, H., Fichtner, H., Frisch, P., Funsten, H., Fuselier, S., Gloeckler, G., Gruntman, M., Izmodenov, V., Knappenberger, P., Lee, M., Livi, S., Mitchell, D., Moebius, E., Moore, T., Reisenfeld, D., Roelof, E., Schwadron, N., Wieser, M., Witte, M., Wurz, P., Zank, G., 2004. The interstellar boundary explorer (IBEX), in physics of the outer heliosphere. In: Florinski, V., Pogorelov, N.V., Zank, G.P. (Eds.), AIP Conference Proceedings, 719; 2004, pp. 162–181.

McComas, D.J., Allegrini, F., Bochsler, P., Bzowski, M., Collier, M., Fahr, H., Fichtner, H., Funsten, H., Fuselier, S., Gloeckler, G., Gruntman, M., Izmodenov, V., Knappenberger, P., Lee, M., Livi, S., Mitchell, D., Möbius, E., Moore, T., Pope, S., Reisenfeld, D., Roelof, E., Scherrer, J., Schwadron, N., Tyler, R., Wieser, M., Witte, M., Wurz, P., Zank, G., 2009a. IBEX—the interstellar boundary explorer. Space Science Review 146, 11–33.

McComas, D.J., Allegrini, F., Bochsler, P., Bzowski, M., Christian, E.R., Crew, G.B., DeMajistre, R., Fahr, H., Fichtner, H., Frisch, P., Funsten, H.O., Fuselier, S.A., Gloeckler, G., Gruntman, M., Heerikhuisen, J., Izmodenov, V., Janzen, P., Knappenberger, P., Krimigis, S., Kucharek, H., Lee, M., Livadiotis, G., Livi, S., MacDowall, R.J., Mitchell, D., Möbius, E., Moore, T., Pogorelov, N.V., Reisenfeld, D., Roelof, E., Saul, L., Schwadron, N.A., Valek, P.W., Vanderspek, R., Wurz, P., Zank, G.P., 2009b. First global observations of the interstellar interaction from the interstellar boundary explorer. Science 326, 959–962.

McComas, D.J., Allegrini, F., Bochsler, P., Frisch, P., Funsten, H.O., Gruntman, M., Janzen, P.H., Kucharek, H., Möbius, E., Reisenfeld, D.B., Schwadron, N.A., 2009c. Lunar backscatter and neutralization of the solar wind: first observations of neutral atoms from the Moon. Geophysical Research Letters 36, L12104.

Möbius, E., Kucharek, H., Petersen, L., Bzowski, M., Saul, L., Wurz, P., Fuselier, S.A., Izmodenov, V.V., McComas, D.J., Müller, H.R., Alexashov, D.B., 2009. Diagnosing the neutral interstellar gas flow at 1 AU with IBEX-Lo. Space Science Reviews 1 (146), 149. doi:10.1007/s11214-009-9495-8.

Niehus, H., Heiland, W., Taglauer, E., 1993. Low-energy ion scattering at surfaces. Surface Science Reports 17 (1993), 213–303.

Scheer, J.A., Wieser, M., Wurz, P., Bochsler, P., Hertzberg, E., Fuselier, S.A., Koeck, F.A., Nemanich, R.J., Schleberger, M., 2005. High negative ion yield from light molecule scattering. Nuclear Instrumentation and Methods B 230, 330–339.

Scheer, J.A., Wieser, M., Wurz, P., Bochsler, P., Hertzberg, E., Fuselier, S.A., Koeck, F.A., Nemanich, R.J., Schleberger, M., 2006. Conversion surfaces for neutral particle imaging detectors. Advances in Space Research 38, 664–671.

Schwadron, N.A., Bzowski, M., Crew, G.B., Gruntman, M., Fahr, H., Fichtner, H., Frisch, P.C., Funsten, H.O., Fuselier, S.A., Heerikhuisen, J., Izmodenov, V., Kucharek, H., Lee, M.A., Livadiotis, G., McComas, D.J., Moebius, E., Moore, T.E., Mukherjee, J., Pogorelov, N.V., Prested, C.L., Reisenfeld, D.B., Roelof, E.C., Zank, G.P., 2009. Comparison of interstellar boundary explorer observations with 3-D global heliospheric models. Science 326, 966. doi:10.1126/science.1180986.

Smith, C.W., Acuña, M.H., Burlaga, L.F., L'Heureux, J., Ness, N.F., Scheifele, J., 1998. The ACE magnetic field experiment. Space Science Reviews 86, 613–632.

Wieser, M., Barabash, S., Futaana, Y., Holmström, M., Bhardwaj, A., Sridharan, R., Dhanya, M.B., Wurz, P., Schaufelberger, A., Asamura, K., 2009. Extremely high reflection of solar wind protons as neutral hydrogen atoms from regolith in space. Planetary and Space Science 57, 2132–2134.

Wurz, P., 2000. Detection of energetic neutral particles, the outer heliosphere: beyond the planets. In: Scherer, K., Fichtner, H., Marsch, E. (Eds.), Copernicus Gesellschaft e.V., Katlenburg-Lindau, Germany, pp. 251–288.

Wurz, P., Fuselier, S.A., Möbius, E., Funsten, H.O., Brandt, P.C., Allegrini, F., Ghielmetti, A.G., Harper, R., Hertzberg, E., Janzen, P., Kucharek, H., McComas, D.J., Roelof, E.C., Saul, L., Scheer, J.A., Wieser, M., Zheng, Y., 2009. IBEX backgrounds and signal to noise. Space Science Review 146, 173–206.